Article

Development of a ^{31}P magnetic resonance spectroscopy technique to quantify NADH and NAD$^+$ at 3 T

Julian Mevenkamp[1,2], Yvonne M. H. Bruls[1,2], Rodrigo Mancilla[2,3], Lotte Grevendonk[2], Joachim E. Wildberger[1], Kim Brouwers[1], Matthijs K. C. Hesselink [2], Patrick Schrauwen[4,5], Joris Hoeks [2], Riekelt H. Houtkooper [6], Mijke Buitinga [1,2], Robin A. de Graaf[7], Lucas Lindeboom[1,2] & Vera B. Schrauwen-Hinderling [1,2,4] ✉

NADH and NAD$^+$ act as electron donors and acceptors and NAD$^+$ was shown to stimulate mitochondrial biogenesis and metabolic health. We here develop a non-invasive Phosphorous Magnetic Resonance Spectroscopy (^{31}P-MRS) method to quantify these metabolites in human skeletal muscle on a clinical 3 T MRI scanner. This new MR-sequence enables NADH and NAD+ quantification by suppressing α-ATP signal, normally overlapping with NADH and NAD$^+$. The sequence is based on a double spin echo in combination with a modified z-Filter achieving strong α-ATP suppression with little effect on NAD$^+$ and NADH. Here we test and validate it in phantoms and in humans by measuring reproducibility and detecting a physiological decrease in NAD$^+$ and increase in NADH induced by ischemia. Furthermore, the ^{31}P-MRS outcomes are compared to analysis in biopsies. Additionally, we show higher NAD$^+$ and lower NADH content in physically active older adults compared to sedentary individuals, reflecting increased metabolic health.

The prevalence of age-related chronic metabolic diseases like obesity, type 2 diabetes, and cardiovascular disease is increasing rapidly worldwide, reaching pandemic proportions[1–3]. It is well known that mitochondrial function is decreased with aging, obesity and type 2 diabetes mellitus[4–6]. The oxidized form of nicotinamide adenosine dinucleotide (NAD$^+$) has been established for a long time to function as an electron acceptor during substrate oxidation and is reduced to NADH during this process. Furthermore, more recently, NAD$^+$ was shown to be an important regulator of mitochondrial biogenesis[7]. During substrate oversupply, which is typical for metabolic diseases, such as type 2 diabetes mellitus, the NAD$^+$/NADH ratio is expected to be lowered[8] hence impacting mitochondrial function. Indeed, a decreased NAD$^+$ bioavailability is reported in both aging and individuals with obesity[9–11] as well as in diabetic mice[12]. In line, high concentrations of NAD$^+$ and a high ratio of NAD$^+$/NADH are both strongly and positively associated with metabolic health[13]. This makes the non-invasive quantification of these metabolites compelling for metabolic research. An overview of some currently available methods to detect NAD metabolites, such as chemical or fluorometric assays or metabolomics, is given in Table 1. All of these methods

[1]Maastricht University Medical Center, Department of Radiology & Nuclear Medicine, Maastricht, The Netherlands. [2]Maastricht University, Department of Nutrition & Movement Sciences (NUTRIM), Maastricht, The Netherlands. [3]Exercise Physiology and Metabolism Laboratory (LABFEM), School of Kinesiology, Faculty of Medicine, Universidad Finis Terrae, Santiago, Chile. [4]Institute for Clinical Diabetology, German Diabetes Center, Düsseldorf, Germany. [5]Leiden University Medical Center, Clinical Epidemiology, Leiden, The Netherlands. [6]Amsterdam University Medical Center, Gastroenterology Endocrinology Metabolism, Amsterdam, The Netherlands. [7]Yale School of Medicine, Department of Radiology & Biomedical Imaging, New Haven, CT, USA. ✉e-mail: v.schrauwen@maastrichtuniversity.nl

Table 1 | Overview of invasive and non-invasive NAD metabolite detection methods

++ = Superior + = Yes or Possible – = No or Not possible	Detects NAD+	Detects NADH	Sensitivity	Detects other NAD-related metabolites	In-situ measurements	Non-Invasive	Sample degradation during processing	Repetitive measurements	Measures absolute concentrations	Whole muscle NAD determination
Biochemical detection										
Fluorometric assays[41]	–	+	+	–	–	–	+	+	+	–
Spectrophotometric assays[41,42]	+	+	+	–	–	–	+	+	+	–
High-performance liquid Chromatography[43]	+	+	+	–	–	–	+	+	+	–
Metabolomics[11]	+	+	+	+	+	–	+	+	+	–
Fluorescence imaging[44–46]	–	+	+	–	+	–	–	+	+	–
MRS										
¹H[25,47]	–	+	–	–	+	+	–	++	+	+
³¹P[14,15,36,37]	+	+	+	+	+	+	–	++	+[a]	+

[a]Currently relative concentrations can be measured, which correlate with absolute concentrations.

require a biopsy to be taken, but in principle, NAD$^+$ and NADH can also be quantified non-invasively by ³¹P-MRS[14]. However, the spectral overlap of α-ATP, NAD$^+$, and NADH resonances in ³¹P spectra so far prohibited the detection of these metabolites in muscle. At high magnetic field[31], P-MRS was successful in quantifying NAD$^+$ and NADH in the brain[15]. However, at clinical field strength and in skeletal muscle, the quantification of NAD$^+$ and NADH has not been demonstrated so far. As mentioned, a complicating factor in the quantification of NAD metabolites is the spectral overlap with the relatively large α-ATP signal. Especially in muscle, where ATP concentrations are higher than in the brain[16,17], this needs to be addressed. As a solution to this problem, spectral editing can be used to manipulate MRS signals based on their individual NMR properties, for example, to suppress certain peaks in the spectrum while leaving other resonances unperturbed. Such an NMR property is homonuclear J-coupling, which causes coupled resonances to split into several peaks in the spectrum and to develop a phase evolution dependent on the used echo time (TE) in spin echoes. α-ATP is a weakly coupled spin system, giving rise to a doublet with a coupling constant of approximately 16 Hz in ³¹P spectra[18]. The coupling of the two phosphate groups in NADH however is unresolved at 3 T, making it appear as a singlet in spectra, while NAD+ in turn appears as a a stongly coupled spin system which again behaves differently from weakly coupled spin systems, such as ATP[18]. Therefore, J-Difference-based editing is a potential approach to differentiate between α-ATP, NADH, and NAD$^+$ by suppressing α-ATP, thereby uncovering NADH and NAD$^+$ resonances in ³¹P-MRS. J-difference editing like MEGA[19] uses a TE of 1/J to invert a J-coupled resonance, whereby J-evolution is refocused in every second acquisition by two frequency selective π RF-pulses. Refocused and inverted coupled resonances from these acquisitions cancel each other out after averaging. However, as we assume NAD resonances to have a relatively short T_2 constant, this approach would lead to strong NAD signal loss.

Therefore, we used a double spin echo (SE) followed by a modified z-Filter as described by Sørensen et al.[20] after a double SE. This sequence was shown to be able to select homonuclear coupled spins based on their coupling constants and allows e.g., the suppression of spins with an even number of coupling partners. However, this previous work used a TE equal to 1/J, similar to MEGA editing, which would result in increased signal loss. We modified the aforementioned sequence so that the J-coupling-based selection mechanism also works with TE equal to 1/2 J, resulting in a single shot suppression for J-coupled spins with TE = 1/2 J. Moreover, we are using a double echo instead of a regular spin echo to create the J-modulation during TE.

Our new sequence was tested and optimized in phantoms with additional optimization in humans while measuring NAD$^+$ and NADH content, relative to intensity of the gamma-ATP resonance in the lower leg. The new sequence was then validated in a proof of principle experiment in eight volunteers during rest and during ischemia, as it is well known that ischemia increases NADH and decreases NAD$^+$ concentrations[21]. Lastly, we performed a cross-sectional comparison of skeletal muscle NAD$^+$ and NADH in older adult individuals with different habitual physical activity levels.

Results
The new editing sequence, designed to suppress α-ATP, is shown in Fig. 1.

Proof of principle in phantoms
Figure 2A, B shows a comparison between an FID and DEMz spectra acquired from a phantom containing ATP and NAD$^+$. DEMz effectively suppressed the α-ATP resonance at 7.52 ppm by 85%, uncovering the NAD$^+$ resonance at 8.46 ppm. The signal loss of NAD$^+$ between FID and DEMz spectra was 22.9%.
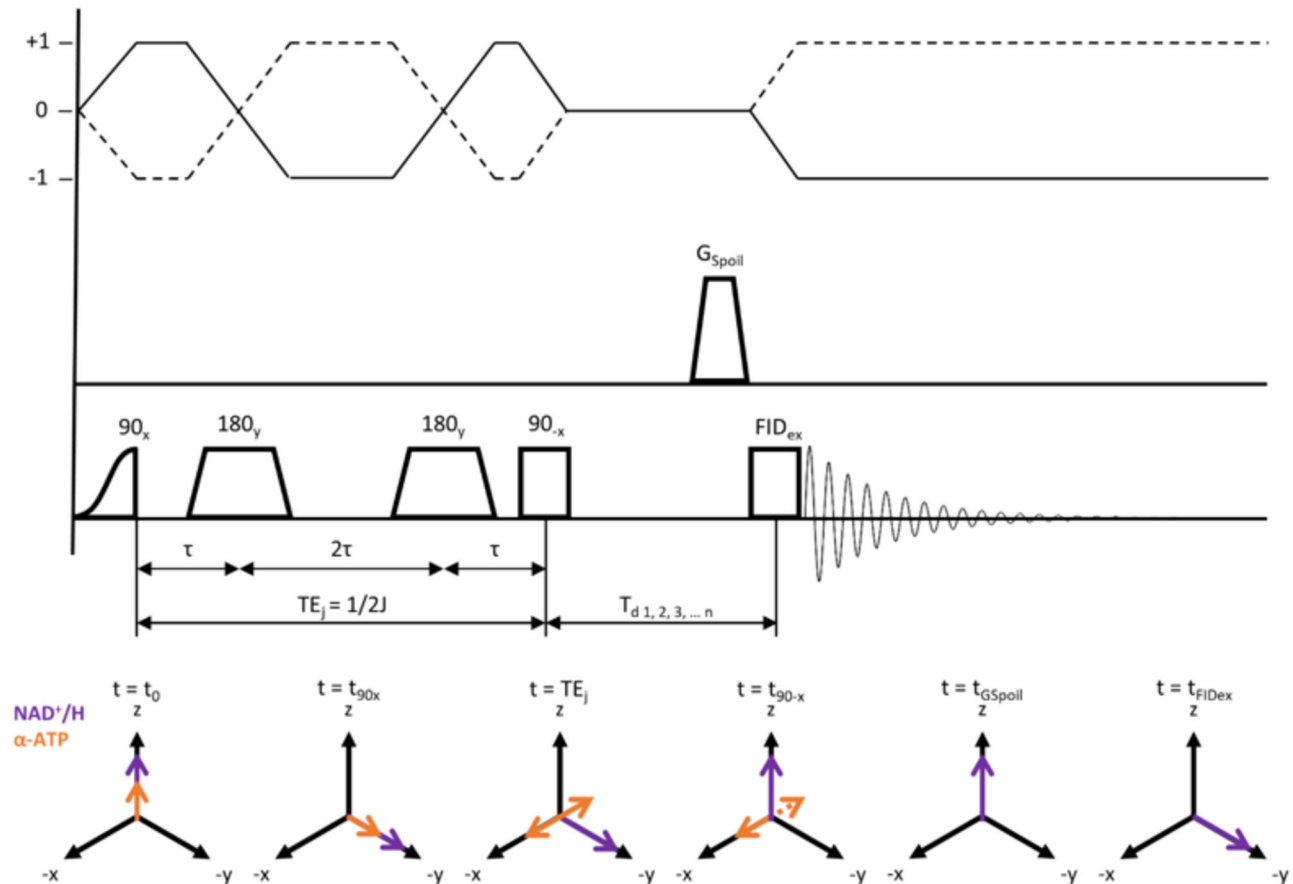
Fig. 1 | Scheme of the double echo modified z-Filter (DEMz) sequence as used in the current approach. After an initial adiabatic half passage hard pulse and two adiabatic full passage pulses, J-coupled α-ATP spins acquire a phase of 90° with respect to uncoupled spins at $t = TE_j = 1/2J$ and end up aligned with x ($t = TE_j$). At t_{90-x} a non-selective 90° block pulse flips spins with J-coupling constants different from that of α-ATP about the x-axis back towards the z-axis. Spins remaining in the x–y plane are then dephased by G_{Spoil}. A varying delay reduces potential phase distortions caused by zero quantum coherences (ZQC).

Concentration ranges of NADH and NAD⁺ in phantoms

Results of fitting DEMz spectra acquired from concentration ranges of NADH and NAD⁺ show an excellent linear correlation (R^2NADH: 0.99 and R²NAD+: 0.99) of fitted relative concentrations and actual molar concentration as displayed by Fig. 2C–D.

Confirming optimal TEj for α-ATP suppression

Figure 2E, F shows a series of TE_j acquired from phantoms with either ATP and NADH or ATP and NAD⁺. The lowest residual α-ATP resonance intensity is thereby achieved with a TE_j of 27.5 ms. Moreover, NADH and NAD⁺ resonance intensities remain constant over the range of TE_j.

α-ATP suppression and NAD detection

Figure 3 shows a comparison of acquired ³¹P MRS FID and DEMz spectra from the muscles of the lower leg. Looking at the FID, we see α-ATP and NAD metabolites as overlapping resonances, hampering a reliable quantification of the NAD⁺ and NADH peaks in the unsuppressed FID spectrum (Fig. 2C). DEMz, however, effectively suppressed the α-ATP resonance on average by 84%. This uncovered the NAD⁺ and NADH resonances (Fig. 2D), which improved the fit for these resonances, as indicated by the lower average relative Cramer-Rao lower bound values listed in Table 2.

Reproducibility measurements

Reproducibility tests of NAD metabolite quantification using DEMz before and after repositioning showed a coefficient of variation (CV) of 7.5% ± 3.0% for fitted NAD⁺ amplitudes (1.1 ± 0.1 Arb. Units) between both acquisitions. The sum of NADH and NAD⁺ showed a CV of 5.5% ± 2.6% (1.4 ± 0.1 Arb. Units), NADH a CV of 21.8% ± 7.6% (0.3 ± 0.1 Arb. Units) and the ratio of NAD⁺/NADH a CV of 23.3% ± 9.4% (4.8 ± 1.6).

Proof of principle in humans: Detecting ischemia-induced changes in NADH and NAD⁺

Eight healthy young lean male ($n = 6$) and female ($n = 2$) volunteers who had no history of coagulation defects and anticoagulant use, were included in the study. All participants had a sedentary lifestyle and did not engage in regular physical activity. No drop-outs or adverse events were reported. All participant characteristics are summarized in Table 3.

When comparing measurements at baseline during rest and during local ischemia in muscles of the lower leg, we detected changes in NADH and NAD⁺ content as shown in Fig. 4. As expected for ischemia, NADH content significantly increased (baseline: 1.53 ± 0.42; ischemia: 1.82 ± 0.36, $p = 0.037$) after a period of ischemia, while NAD⁺ content decreased (baseline: 4.16 ± 0.74; ischemia: 3.16 ± 0.55, $p = 0.004$). Consequently, this resulted in a reduced NAD⁺/NADH ratio (baseline: 2.81 ± 0.52; ischemia: 1.82 ± 0.54, $p = 0.004$).

Cross-sectional comparison of NADH and NAD⁺ in older adults

To test whether the newly developed MRS sequence can detect physiologically relevant differences in NAD⁺ and NADH, we assessed NAD⁺ and NADH content in the skeletal muscle of normally active men and women ($n = 8/7$) (OA) and exercise-trained older men and women ($n = 7/6$) (OT), anticipating a higher NAD⁺ content in OT when
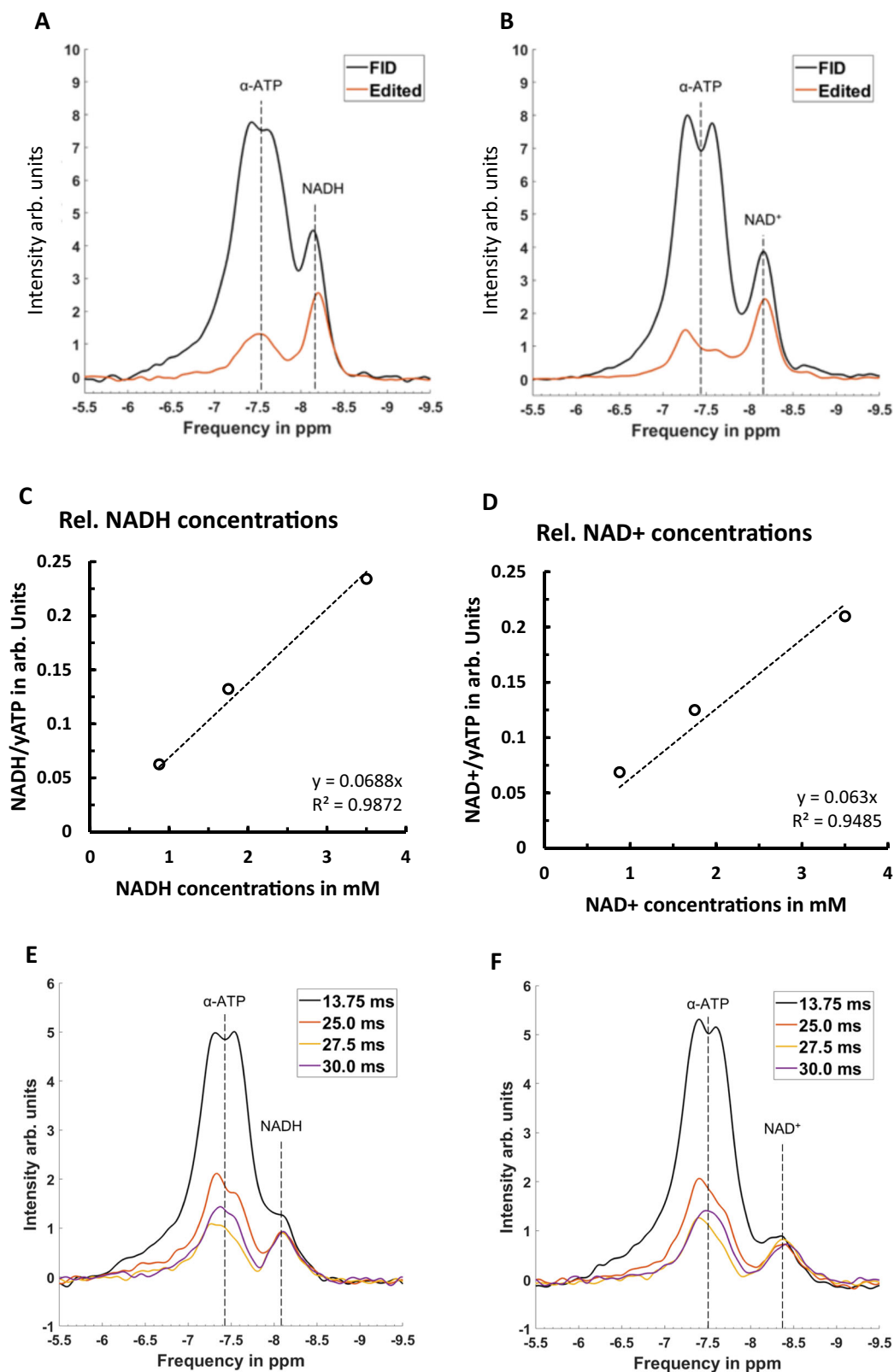
Fig. 2 | Comparison of spectra resulting from FID and DEMz acquisition in phantoms. Phantoms composed of ATP and NADH (**A**) or ATP and NAD$^+$ (**B**) were measured. α-ATP suppression of 85% with an approximate signal loss of 22.7% for NADH and 22.9% for NAD$^+$ were observed. Relative concentrations resulting from DEMz spectra of NADH (**C**) and NAD$^+$ (**D**) phantoms over actual NADH and NAD$^+$ concentrations of phantom compartments in mM are shown. In **E** and **F**, a series of editing echo times (TE$_j$) of 13.75 ms, 25.0 ms, 27.5 ms, and 30.0 ms in double echo modified z-Filter (DEMz) sequence measuring a phantom composed of 5 mM ATP and 3.5 mM NADH (**E**) and a phantom with 5 mM ATP and 3.5 mM NAD$^+$ (**F**) are shown. NADH resonance intensity remains stable over this range of TE$_j$. α-ATP residual is smallest at TE$_j$ 27.5 ms. Similarly, results were observed on the NAD$^+$ resonance. Source data for **C**, **D** are provided as a Source Data file.
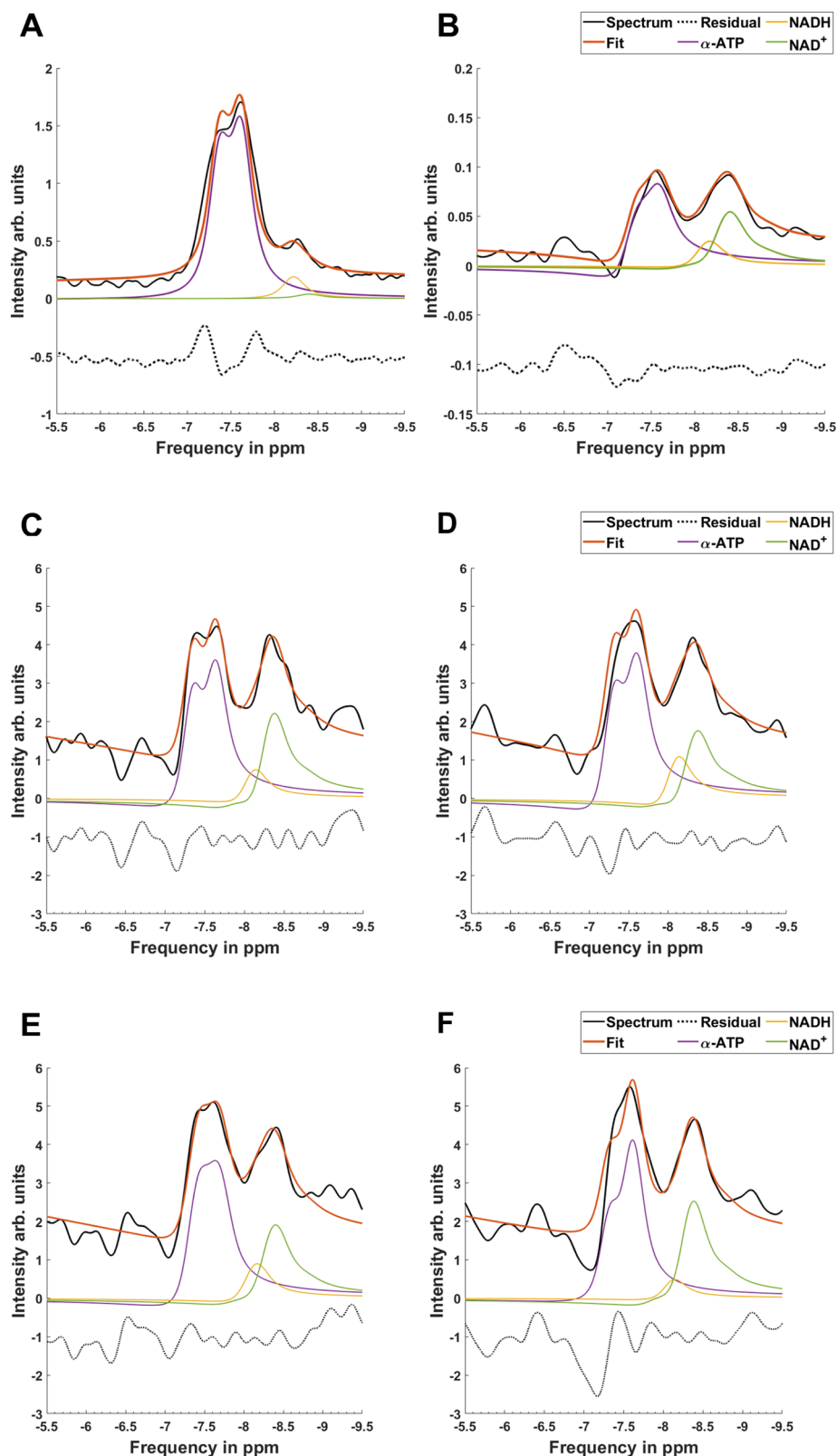
Fig. 3 | Comparison between NAD⁺ and NADH fitting. Fitting results from FID (**A**) and DEMz spectra (**B**) are shown. Moreover, DEMz spectra measured during rest (**C**) and during 9 min of ischemia (**D**) in the same participant as well as from a normally active older adult (**E**) and a trained older adult (**F**) are shown. Spectra from older trained and normally active adults were normalized by their respective intensities of γ-ATP. Comparing **A** and **B** shows the increased separation of NAD⁺ and NADH resonances from α-ATP in DEMz spectra compared to FID. Ischemia visibly lowers the NAD⁺/NADH ratio, as shown in the comparison of (**C**) and (**D**). Normally active older adults display overall lower NAD⁺ and NADH content and lower NAD⁺/NADH ratios than older trained adults, as depicted by (**E**) and (**F**). First-order phase and phase artefacts on the edited α-ATP resonance are incorporated into the fitting model, as described in the "Methods" section under "Spectral analysis".

Table 2 | Average relative Cramer Rao lower bounds of fits from FID and DEMz spectra for NADH, NAD⁺, PCr, and γ-ATP

CRLB in %	NADH	NAD⁺	PCr	γATP
FID	15.96 ± 3.88	10.73 ± 3.43	0.28 ± 0.03	0.33 ± 0.02
DEMz	9.76 ± 1.74	3.85 ± 0.71	0.27 ± 0.06	1.5 ± 0.31

Values are reported as mean ± SEM.

Table 3 | Participant characteristics at screening for detecting ischemia-induced changes by ³¹P-MRS DEMz

Variable	Healthy lean young participants (n = 8)
Gender (m/f), n	6/2
Age (y)	28 ± 2
Body weight (kg)	71.5 ± 3.2
Body mass index (kg/m²)	22.9 ± 0.5
Fat mass (kg)	19.2 ± 2.7
Fat-free mass (kg)	52.3 ± 3.6
Fat percentage (%)	27.0 ± 3.5
Systolic blood pressure (mmHg)	116 ± 4 (<120)
Diastolic blood pressure (mmHg)	71 ± 2 (<80)
Creatinine (μmol/L)	79.8 ± 2.9 (60–115)
ASAT (U/L)	21.8 ± 1.4 (<35)
ALAT (U/L)	15.9 ± 1.3 (<45)
PT (s)	11.35 ± 0.12 (11–13.5)
aPTT(s)	29.5 ± 0.5 (30–40)
INR	1.08 ± 0.01 (0.8–1.1)

Data are presented as mean ± SEM. *ASAT* aspartate aminotransferase, *ALAT* alanine aminotransferase, *PT* prothrombin time, *aPTT* partial thromboplastin time, *INR* international normalized ratio. Normal values in parentheses.

compared to OA[7,13,22]. The determination of PCr recovery kinetics confirmed increased physical fitness of OT compared to OA as the halftime of PCr recovery was significantly lower in OT (17.11 s ± 4.2 s vs. 23.7 s ± 6.5 s, $p < 0.01$). BMI was significantly lower in OT than in OA (23.5 kg/m² ± 2.0 kg/m² vs. 26.2 kg/m² ± 2.7 kg/m², $p < 0.05$), whereas lean body mass was comparable (50.7 kg ± 9.8 kg vs. 50.5 kg ±10.1 kg, $p > 0.05$). The participants were asked back from a previous study of our group, where they were extensively characterized and [23] their screening results are depicted in Table 4.

By applying the ³¹P-MRS DEMz sequence, significantly lower NADH content was detected in OT than in OA (1.16 ± 0.13 vs. 1.71 ± 0.12, $p = 0.006$), (Fig. 5a) whereas significantly higher NAD⁺ content was detected in OT (5.58 ± 0.22 vs. 4.42 ± 0.17, $p = 0.0003$), as well as higher NAD⁺/NADH ratios (5.61 ± 0.64 vs. 2.84 ± 29, $p = 0.001$) compared to OA (Fig. 5b, c). Total NAD metabolite content exhibited borderline significantly higher values in OT compared to OA (6.75 ± 0.21 vs. 6.13 ± 0.2, $p = 0.051$) (Fig. 5d). Values were reported as ratios relative to measured γ-ATP intensities, as these are considered as constant in muscle tissue[24].

Biopsy vs. MRS

So far, analysis of muscle biopsy material has been the only possibility to obtain data on NADH and NAD+ in humans. Here we compared MRS-based NAD(H) metabolites with data obtained in small muscle biopsies obtained from the vastus lateralis, immediately samples after the MRS measurements. These comparisons are shown in Fig. 6. There is good agreement between the quantification of NADH with both methods. The agreement of NAD+ is less strong, however, agreement for NADH/NAD+ ratio and for the sum of NAD metabolites is again good.

Discussion

We here showed that with edited ³¹P MRS, based on a **D**ouble **E**cho **M**odified **z**-Filter (DEMz), it is possible to suppress α-ATP and thereby uncover NAD⁺ and NADH resonances on a clinical 3 T MR scanner. This approach allows the observation of NAD⁺ and NADH in skeletal muscle in a completely non-invasive way, without performing a biopsy.

We tested the performance of the sequence in phantoms and in humans and showed that we could reach strong suppression of α-ATP while sparing the NAD⁺ and NADH signal as anticipated. In fact, 85% of the ATP signal was suppressed, while only 23% of NADH and NAD⁺ signal intensity was lost in phantom tests. Comparable α-ATP suppression was achieved in humans.

Previous studies focusing on the non-invasive quantification of NAD metabolites focused on the brain only and used MR scanners with magnetic fields above clinically used field strength. High-field MR scanners provide a significant advantage over clinical field strength due to their superior spectral resolution, which allows for the direct quantification of NAD+ and NADH metabolites in the ³¹P-spectrum, as exemplified in brain tissue[14,15]. Nevertheless, the broad use of this technique is challenged by the limited accessibility and high expenses associated with high-field MR. Therefore, our objective was to develop a sequence capable of measuring NAD+ and NADH metabolites at clinical field strength.

Detecting NAD metabolites in skeletal muscle using MR spectroscopy is more challenging when compared to the brain. In skeletal muscle, the ATP concentration is more than twofold higher than in brain tissue[17], resulting in a larger contamination of NAD resonances by ATP. Moreover, achieving magnetic field homogeneity through B_0 shimming is more difficult in in the muscle compared to the brain, generally leading to broader linewidths and increased signal overlap. Efforts to further enhance spectral resolution at lower field strength involved the utilization of ¹H decoupling in ³¹P spectra[14]. Despite the promising results reported in the brain[14]. Furthermore, saturation transfer effects from water to NAD⁺ reduce the visible amount of NAD⁺ in ¹H MRS spectra, and relatively long scan durations are necessary to compensate for the low SNR[25], leaving ³¹P-MRS as the most promising approach to detect NAD⁺ and NADH resonances in skeletal muscle.

In this article, we propose to overcome some of the above-mentioned drawbacks by selectively suppressing the α-ATP resonance using DEMz. This selective suppression of α-ATP uncovers the NAD+ and NADH resonances allowing a more accurate quantification of these resonances. With his sequence, we were able to obtain an 85% reduction of the α-ATP resonance, both in phantoms and in human volunteers, enabling the quantification of both NAD+ and NADH. In phantoms, the detected NAD+ and NADH concentrations correlated very well with known phantom concentrations, demonstrating the quantitative nature of this approach. That this sequence offers a more accurate quantification of NAD resonances than conventional ³¹P-MRS was further illustrated by the lower Cramer Rao lower bounds (CRLB) for NADH and NAD⁺, when comparing the two methods. Reproducibility measurements further confirmed the robustness of this method with CVs of <10% for NAD⁺ and for the sum of NAD⁺ and NADH. Due to the lower concentration of NADH, the detection of NADH content is more challenging as reflected by a higher CV of 23%. Nevertheless, significant differences in NADH were detected during the proof-of-concept experiment in ischemia, showing that the method is able to pick up physiological differences in NAD⁺ as well as NADH.

Although the NAD+ and NADH resonances are unaffected by the J-coupling-based editing scheme, we did observe a 23% decrease in the NAD+ and NADH signal in our phantom studies. We believe that this is due to a combination of B1 inhomogeneity and T_2 decay during TE of the double spin echo. One potential method to enhance B1 homogeneity and SNR could be the use of half volume coils in combination with quadrature detection[26], however such coils are not broadly

A

B

C
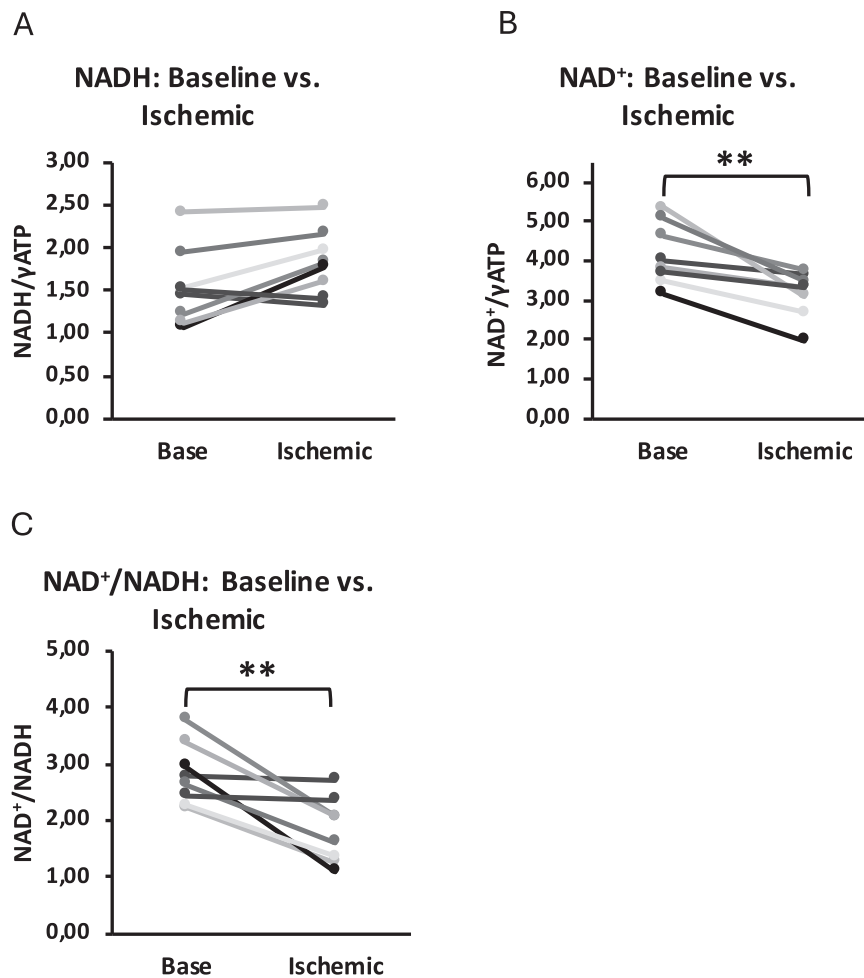
Fig. 4 | Validation of the 31P-MRS editing sequence. To test and validate the 31P-MRS editing sequence, we performed the measurement during normal perfusion of the muscle and during ischemia. Here, we show changes from baseline to ischemic state of NADH contents (**A**), NAD⁺ content (**B**), and ratios of NAD⁺/NADH (**C**) in the calf muscle of eight healthy young volunteers ($n = 8$). Changes were statistically tested using a two-sided paired student t-test. **A** $p = 0.037$, **B** $p = 0.004$, **C** $p = 0.004$. ** $p < 0.01$, * $p < 0.05$.

available at this point in time, which would hamper broad dissemination of the method.

The ATP suppression that is currently reached is not absolute, and we assume that remaining ATP signals originates from T_1 relaxation during the spoiler delay. The current (non-complete) suppression of ATP however appears to be sufficient to uncover and quantify NAD metabolites, while sparing NAD+ and NADH signal intensity. A future
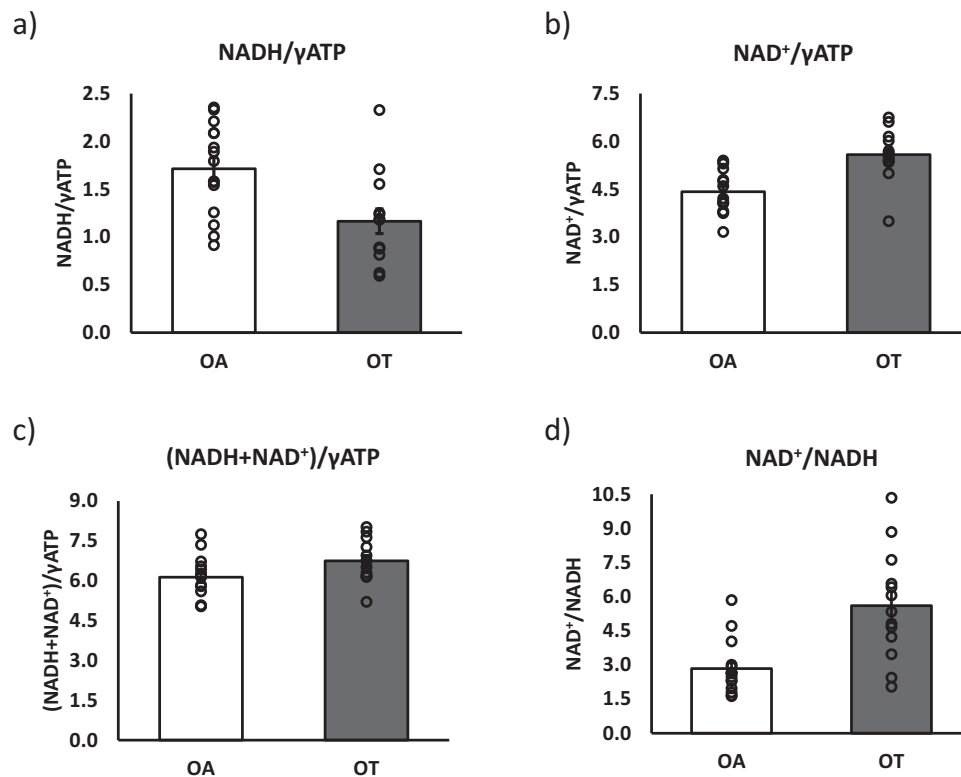
Table 4 | Screening results of normally active and trained older adults undergoing NAD MRS

Variable	Normally active older adults (OA) ($n = 15$)	Trained older adults (OT) ($n = 13$)	p-Value
Gender (m/f), n	8/7	7/6	
Age (y)	72 ± 4	68 ± 2	<0.01
Body weight (kg)	76.9 ± 8.0	67.4 ± 8.7	<0.05
Body mass index (kg/m²)	26.2 ± 2.7	23.5 ± 2.0	<0.05
Fat mass (kg)	26.5 ± 8.6	16.7 ± 5.2	<0.01
Fat-free mass (kg)	50.5 ± 10.1	50.7 ± 9.8	>0.05
Fat percentage (%)	34.5 ± 10.6	25.1 ± 8.5	<0.01
PCr recovery half-time (s)	23.7 ± 6.5	17.11 ± 4.2	<0.01

improvement to mitigate residual ATP signal originating from T1 relaxation could be the introduction of a two-step phase cycle of the first 90° pulse (x,−x) and receiver phase (x,−x) during signal averaging.

While our method demonstrates the potential for quantification of NAD metabolites by DEMz, sophisticated post-processing analyses is needed to separate NADH and NAD⁺ resonances in a 3 T ³¹P MRS spectrum. Therefore, our quantification approach used strong prior knowledge in the fitting procedure to quantify NAD⁺ and NADH separately. This resulted in excellent quality of the fit, and the robustness of the fit was backed up by a CRLB below 10% for NADH and below 4% for NAD⁺, showing the robustness of the quantification procedure

The editing method presented here allowed us to determine changes in NAD⁺ and NADH during ischemia. However, the observed changes in NAD metabolite content induced by ischemia were somewhat lower in magnitude than what has been previously reported when using biopsy techniques (122% vs. 143%)[21]. A likely explanation for this difference could be the fact that we averaged spectra over a 9-min period immediately after the application of the cuff to induce ischemia. Therefore, during the first part of the MRS measurement, ischemia was not fully present yet, whereas earlier studies involved a biopsy taken precisely at the 10-min mark of ischemia, capturing the NADH content at that specific moment, when ischemia is likely to be more complete. Considering these differences in ischemia protocol, the present results are very well aligned with earlier findings. In two

Fig. 5 | Comparison of NADH and NAD+ content in normal active versus exercise-trained adults. To test whether the method can detect differences between volunteers differing in fitness and metabolic health status, NADH and NAD+ content were assessed in normally active and exercise-trained older adults. Here, we show a comparison of NADH content (**a**), NAD$^+$ content (**b**), total NAD content (**c**), and NAD$^+$/NADH ratios (**d**) in 15 normally active older adults (OA, $n = 15$) and 13 trained older adults (OT, $n = 13$). Data are presented as mean values ± SEM. Groups were statistically compared using a two-sided unpaired student t-test. **a** $p = 0.006$, **b** $p = 0.0003$, **c** $p = 0.001$, **d** $p = 0.051$. ** $p < 0.01$, * $p < 0.05$. Source data are provided as a Source Data file.

participants, we observed a rise in NADH relative concentrations of 6.7% and 7.9%, respectively, during ischemia, which was unexpected. However, this increase lies within the 10% variation of fitted NADH amplitudes as shown by its CRLB and, therefore, falls within the expected variation.

In addition to the proof-of-concept experiment conducted during ischemia, we also performed a cross-sectional comparison of NAD$^+$ and NADH content between highly trained and normally active older adults. As expected, we observed higher NAD$^+$ content in the more active group, consistent with recent findings using biopsies[11]. These results are in line with earlier results in both human and animal models, underscoring the significance of physical activity in preserving NAD$^+$ and NADH content[11].

We also tested the agreement of the MRS method with analysis of biopsy specimens from skeletal muscle. While we found a reasonable correlation between the two methods regarding NADH, the correlation for NAD+ was less strong. It is important to note that at this stage, the comparison of the methods could only be performed in a rather homogenous group of volunteers with respect to metabolic health, as all participants were between 65 and 75 years of age, not physically active, and overweight but otherwise healthy. In a group where the range of values is small, it is more difficult to find a correlation.

Also, it should be noted that muscle biopsies in humans are limited by the size of the biopsy taken, and that within muscle NAD levels can also vary, depending on for example fiber type and mitochondrial content. Indeed, the volume of interest (VOI) observed by our 10 cm surface coil, assuming a half-spherical B1 is used in MRS, is ~50,000 times larger than the ~5 mg of muscle material from biopsy. Importantly, the comparison between

groups of differing metabolic health that we also present shows that the MRS method is sensitive enough to pick up clinically significant differences. Indeed, we found differences in NADH and NAD+ between physically trained individuals when compared to normally active people and these differences are in agreement with earlier analysis in muscle biopsies[11]. Also, the validation of our MRS method in phantoms was very good, and the reproducibility was good to high. Therefore, the MRS method is sensitive enough to detect differences between groups, even based on lifestyle only. This holds promise to detect differences between healthy volunteers and patients with metabolic disease.

In conclusion, DEMz is a feasible approach for the detection of NAD$^+$, NADH, and acute changes in relative NADH and NAD$^+$ concentrations, and we could pick up physiological changes as they occur during ischemia and physiological differences between groups of differing metabolic health. However, the visible spectral resolution of NADH and NAD$^+$ resonances remains challenging, but the separation of the two resonances could be achieved by using a fitting algorithm with strong prior knowledge. Absolute concentrations of NAD metabolites can be calculated in the future, once T$_2$ relaxation times are established that allow the respective T$_2$ correction. To our knowledge, this is the first non-invasive method to determine NAD$^+$ and NADH in skeletal muscle, and importantly, this was achieved at clinical field strength.

Methods
Development of the ³¹P MRS double echo modified z-Filter sequence
As outlined above, α-ATP represents a homonuclear weakly coupled two-spin system wherein an MRS phenomenon called
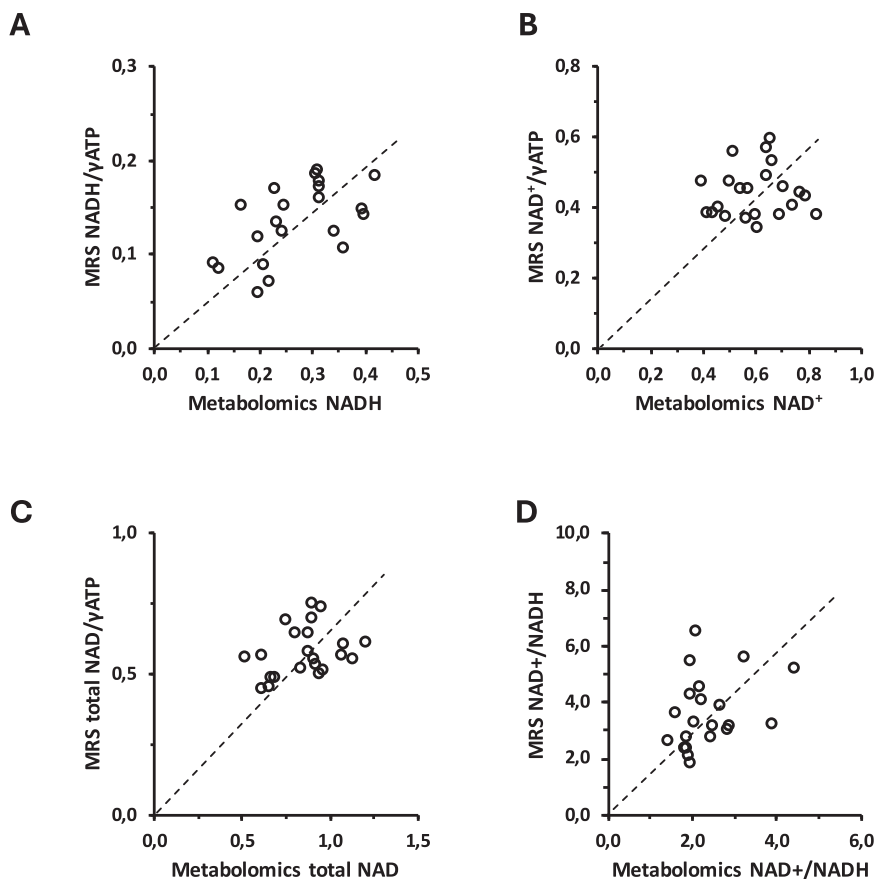
Fig. 6 | NAD metabolism by metabolomics versus MRS. NADH (**A**), NAD⁺ (**B**), NAD⁺/NADH ratio (**C**), and total NAD (**D**) quantified by metabolomics plotted against their respective MRS results and trend line (stippled line). Source data are provided as a Source Data file.

J-coupling arises, which can be used for spin selection by spectral editing. The effects of J-coupling become visible in a spin echo as coupled spins undergo a phase evolution based on TE and their coupling constants[18,27,28]. The following equations make use of the product operator formalism[29] and will show the principle of our new editing sequence designed to suppress α-ATP, which is shown in Fig. 1.

Equation 1 describes the initial rotation of a spin system with one coupling by a 90⁰ excitation about the x-axis from equilibrium into the x-y plane, see also $t = t_{90x}$ in Fig. 1:

$$I_{1z} + I_{2z} \xrightarrow{(\frac{\pi}{2})(I_{1x} + I_{2x})} -(I_{1y} + I_{2y}) \tag{1}$$

Equation 2 describes the J-evolution of a homonuclear coupled two-spin system in a double echo sequence with a total TE equal to 4τ (see Fig. 1),

$$-(I_{1y} + I_{2y}) \xrightarrow{(\pi J 4\tau) I_{1y} I_{2y}} -(I_{1y} + I_{2y})\cos(\pi J 4\tau) + 2(I_{1x}I_{2z} + I_{1z}I_{2x})\sin(\pi J 4\tau) \tag{2}$$

If $4\tau = 1/2J$ in Eq. 2, we can see that the coupled α-ATP spins acquire a phase of $\pm\frac{\pi}{2}$ with respect to the frame of reference[27] and end up as antiphase terms:

$$-(I_{1y} + I_{2y}) \xrightarrow{(\pi J \frac{1}{2J}) I_{1y} I_{2y}} -(I_{1y} + I_{2y})\cos\left(\frac{\pi}{2}\right) + 2(I_{1x}I_{2z} + I_{1z}I_{2x})\sin\left(\frac{\pi}{2}\right) \tag{3}$$
$$= 2(I_{1x}I_{2z} + I_{1z}I_{2x})$$

Furthermore, coupled spins with different J-constants than α-ATP will retain a y-component next to the antiphase term as for them:

$$-\left(I_{1y} + I_{2y}\right)\cos\left(\pi J \frac{1}{2J_{\alpha ATP}}\right) \neq 0 \tag{4}$$

Where the antiphase terms of coupled spins with $J \neq J_{\alpha ATP}$ will lead to zero quantum coherences (ZQC) and, therefore, phase distortions of the acquired spectrum. As a solution, acquisitions with alternating delays (T_d) between editing and FID acquisition lead to phase evolution of ZQC, which eventually leads to their cancellation after averaging multiple acquisitions with varying phase states[30,31]. Other spins that still have a y-component, e.g., uncoupled spins that only underwent chemical shift evolution during TE, will be fully refocussed after the two 180 pulses:

$$I_z \xrightarrow{(\frac{\pi}{2})I_x} -I_y \xrightarrow{(2\pi)I_y} -I_y \tag{5}$$

Those y-components will feel the effect of the 90°$_{-x}$ pulse and end up with magnetization returned to equilibrium, see Fig. 1 $t = t_{90-x}$:

$$-I_y \xrightarrow{(-\frac{\pi}{2})I_x} I_z \tag{6}$$

At this point, $t = G_{spoil}$, a spoiler gradient dephases all magnetization still present in the transversal plane before the subsequent FID at $t = t_{FID}$ excites spins previously returned to equilibrium, ultimately removing α-ATP spins from the observable magnetization.

The new **D**ouble **E**cho **M**odified **z**-Filter (DEMz) sequence was implemented on a multi-nuclei clinical scanner (Achieva 3T-X, Philips Healthcare, Best, The Netherlands) and first tested in a two-compartment phantom, containing ATP and NAD^+. Second, the reproducibility was determined in humans, whereafter a proof of principle experiment investigated whether the measurement is sensitive enough to detect physiological changes induced by ischemia. Finally, the sequence was applied in groups differing in metabolic health to investigate differences in NAD^+ and NADH. A 10 cm single loop ^{31}P-MRS coil (P100, Philips Healthcare, Best, The Netherlands) was used in all measurements. RF pulse shapes and durations are given in Supplementary Table S1. The specific absorbance rate (SAR), according to the calculations of the MR system, was <7.3 W/kg, which is well below the limit of 20 W/kg for extremity scans.

Testing of the ^{31}P-MRS DEMz sequence in phantoms
To quantify the accuracy of the ^{31}P-MRS DEMz sequence, we prepared two compartment phantoms with NAD^+ and NADH compartments of 0.875 mM, 1.75 mM, and 3.5 mM of NADH and, respectively, NAD^+. The exact composition of the phantoms is listed in supplementary Table S2. Signal loss of NADH and NAD^+ caused by spectral editing was determined in the phantom with the highest concentration (3.5 mM).

Firstly, an FID of these phantoms was acquired for reference with NSA = 32, points=2048, BW = 3000 Hz, and TR = 4000 ms. Secondly, DEMz spectra were acquired with: NSA = 32, points = 2048, BW = 3000 Hz, $TE_j = 27.5$ ms, TR = 4000 ms and $T_{d\ Start} = 11.25$ ms, $T_{d\ End} = 29.25$ ms, $n_{Td} = 8$, T_d step = 2.25 ms and eight step phase cycling. By comparing the signal intensities of α-ATP and NAD^+ in the edited spectrum to the reference spectrum, we determined the relative suppression of α-ATP and signal loss of NADH and NAD^+.

Moreover, the two compartment phantoms with 3.5 mM NADH and the phantoms with 3.5 mM NAD^+ were used to measure a range of TE_j to confirm that the chosen TE_j of 27.5 ms is optimal for α-ATP suppression. For this purpose, we used the DEMz sequence with identical settings as mentioned above, however we increased TE_j from the shortest possible value of 13.75–25.0 ms, 27.5 ms, and finally 30.0 ms.

Measurements in humans
Ethical approval. For all measurements in humans, participants provided written informed consent, and study protocols were approved by the local medical ethical review committee of Maastricht University. The use of the metabolomics data for this study was also approved by the local medical ethical review committee of Maastricht University. All studies were conducted in compliance with the Declaration of Helsinki. Trial monitoring was performed by the Clinical Trial Center in Maastricht, The Netherlands. The studies were registered at the Netherlands trial register with the identifier NL8888 and at clinicaltrials.gov with identifiers NCT03666013 and NCT04907110. Only baseline data was used from the study registered under NCT04907110.

MRS acquisition protocol. For all measurements in humans, the same MRS protocol was used. A 10 cm single-tuned ^{31}P surface coil (Philips Health Care, Best, the Netherlands) earlier used in the phantom experiments was also used in humans. Participants were positioned supine and feet first with their calf resting upon the coil. Non-localized FIDs of the participants were acquired from the calf muscles with NSA = 32, points = 2048, BW = 3000 Hz, and TR = 4000 ms. Subsequently, DEMz spectra were acquired. Scan parameters in rest: NSA = 128, points = 2048, BW = 3000 Hz, TR = 4000 ms, $TE_j = 27.5$ ms, $T_d = n/(-f_{\beta ATP}\text{-}f_{\alpha ATP})$ with n = 1…32, equal to $T_{d\ 1, 2, 3… 32} = 11.25$ ms, 13.5 ms, 15,75 ms…81 ms. Moreover, all spectra were acquired with eight-step phase cycling.

Determination of reproducibility
The reproducibility of the DEMz sequence was tested in five individuals by performing two repeated measurements with repositioning between the measurements. The acquired spectra were fitted individually, as described later, and the coefficient of variation (CV) of NADH and NAD+ was determined.

Detection of changes in humans, during ischemia
To test and validate the ^{31}P-MRS editing sequence, we performed the measurement during normal perfusion of the muscle and during ischemia. As there is no oxygen supply during ischemia, NADH cannot be oxidized to NAD^+ by the electron transport chain, leading to an accumulation of NADH and a drop of NAD^+ in the cell[21]. This acute change in NAD metabolite concentrations was shown earlier in biopsies, where a peak of NADH accumulation occurred after about 10 minutes[21]. We chose our study design based on this approach and monitored NAD^+ and NADH during normal perfusion and during ~9 min of ischemia, which is equivalent to an NSA of 128 with TR 4000 ms.

Participants
All participants recruited for this study provided written informed consent. The study was registered at the Netherlands trial register with identifier NL8888. Eight healthy lean (BMI: 18–25 kg/m², age: 18–40 years) male (n = 6) and female (n = 2) (self-reported gender) participants were included. Exclusion criteria were MRI-contraindications, uncontrolled hypertension, impaired liver function, kidney insufficiency, engagement in exercise for more than 3 h per week, unstable body weight (weight gain or loss more than 5 kg in the previous 3 months), excessive alcohol consumption (males > 4 units/day, females > 3 units/day), use of anti-coagulants, and use of other medication known to interfere with the outcome parameters/patient safety. Coagulation, kidney and liver functions were assessed by blood sample analysis for prothrombin time (PT), partial thromboplastin time (aPTT), international normalized ratio (INR) creatinine, aspartate aminotransferase (ASAT), and alanine aminotransferase (ALAT).

Experimental design
All participants reported to the university in the morning after an overnight fast of at least 10 h. Participants refrained from alcohol and strenuous physical activity 3 days prior to the test day. During the test day, body composition was determined with a Bod Pod device (Cosmed, Italy, Rome) using air–displacement plethysmography[32]. Thoracic gas volume was predicted based on equations included in the Bod Pod software. From these data, body fat-free mass, fat mass, and fat percentage were calculated as described by Siri[33]. Subsequently, skeletal muscle NAD^+ and NADH concentrations were determined under normal perfusion and during ischemia using the new ^{31}P-MRS DEMz sequence as described under the MRS acquisition protocol. Ischemia was applied by inflating an MR-compatible blood pressure cuff (to 50 mmHg above the resting systolic pressure determined prior to the start of the MRS measurement) placed around the upper leg of the participant, and the measurements were repeated during ischemia.

Cross-sectional NAD metabolite comparison
To test whether the method can detect differences between volunteers differing in fitness and metabolic health status, NADH and NAD^+ content were assessed in normally active men and women (n = 8/7) (OA) and exercise-trained older men and women (n = 7/6) (OT), who participated in one of our previous studies[23], which also provided screening results such as body composition by body plethysmography, age, and self-reported gender. All participants recruited for this study provided written informed consent. This study was registered at clinicaltrials.gov with the identifier NCT03666013.

Inclusion in the previous study was based on self-reported activity levels. The untrained group did not exercise for more than one hour per week, while the trained volunteers participated in at least three structured exercise sessions per week. For this study, participants came to the University for one test day on which NAD metabolites were measured by using our new ^{31}P MRS DEMz editing sequence under resting conditions. Subsequently, following the NAD measurement, a dynamic ^{31}P MRS during exercise was performed in the scanner in order to determine PCr recovery kinetics as a measure of oxidative capacity for training status characterization according to ref. 34.

Comparing MRS to metabolomics

All participants provided written informed consent. This study was registered at clinicaltrials.gov with the identifier NCT04907110. Only baseline data was used for the present study. Spectra were acquired with the above-mentioned protocol but with a 10 cm surface coil placed on the m. vastus lateralis in 24 elderly, normally active/sedentary individuals with overweight/obesity (age 65–80 years, BMI: 25–35 kg/m^2). Subsequently, skeletal muscle tissue samples were taken from each participant via needle biopsy from m. vastus lateralis as described by Bergström et al.[35]. Muscle tissue samples were immediately frozen and stored at −80° until analysis. Samples were analyzed in batches by metabolomics as described earlier[11]. Metabolomics gives insight into different NAD metabolites such as NADH, NAD+, and NADP+. For the correlation of biopsy and MRS results, NAD+ and NADP+ concentrations were summed, and likewise, NADH and NADPH were summed when compared to the fitted NAD+ and NADH signal in 31P-MR-spectra as these resonances cannot be distinguished in humans[36]. MR-spectra was analyzed as described in the following section.

Spectral analysis

Spectra were fitted with an in-house developed MATLAB script (MATLAB 2018b, The MathWorks, Inc.), using extensive prior knowledge, such as relative chemical shifts of metabolites, T_2 values, amplitude starting values, amplitude relationships between resonances, the multiplicity of peaks and first-order phase (see Supplementary Table S3). Additionally, homonuclear J-coupling constants for α- and γ-ATP resonances were determined from reference FIDs individually and added to the prior knowledge to ensure a better fit of these resonances. α-ATP's coupling constants are also crucial for fitting phase deviations of residual α-ATP in DEMz spectra, which occurs when α-ATP magnetization is not aligned with the *x*-axis before the second 90° pulse in the case of TE$_j$ ≠ 1/2 J.

To accommodate for the expected phase deviation caused by individual α-ATP J-coupling constant not meeting the condition TEJ = 1/2 J, we calculated the phase deviation according to the following equation and added it to the fitting model for the α-ATP resonance:

$$\Delta\phi_J = 2\pi \cdot TE_j \cdot \Delta J$$

$$\Delta J = 18.18 Hz - J_{Measured}$$

$$TEJ = 27.5{}^{*}10^{\wedge} - 3\,s''$$

Furthermore, homonuclear coupling patterns of NAD+ resonances were added to the fitting model. NAD+ was modeled as a strongly coupled quartet based on the findings of Lu et al.[37]. The chemical shift between the two NAD+ resonances at 3 T was also calculated based on Lu et al. and deduced to be 24.43 Hz. α-ATP and γ-ATP were modeled as doublets, of which the respective coupling constants were determined and fitted for each participant individually based on their acquired reference FIDs.

Subsequently, fit parameters such as line width, frequency shifts, zero-order phase, amplitudes, baseline, and (optionally) phase distortions of individual peaks were adjusted to match the acquired spectrum. The code used to analyze the data is publicly available on: 10.5281/zenodo.13834427. The abundance of NAD+ and NADH is either reported as arbitrary units (Arb. Units) in reproducibility measurements or unitless as a ratio relative to γ-ATP in the case of inter-individual comparisons. As ATP is generally assumed to be very constant across populations, these values are directly proportional to molar concentrations. Furthermore, NADH and NAD+ intensities relative to y-ATP intensities will be referred to as NADH or NAD+ content in this article. Calculating absolute concentrations requires correction for T_2 decay during the double spin echo within the DEMz but T_2 values for NAD+ and NADH are unknown, therefore we were unable to calculate absolute concentrations. However, as all data points would have been corrected using the same T_2 values, it has no effect on the final result.

As we used the same TEJ for all measurements, we expect that the signal loss due to the editing sequence was consistent across all participants and conditions (normoxia, ischemia, trained, and sedentary). Potential other variations in signal loss could be based on variations in T2-associated signal loss. However, there is no reason to expect major differences in T2 relaxation times across individuals, as generally, these differences are small, as documented by Bogner et al.[38]. Furthermore, the NAD+ and NADH content is given as a ratio, relative to ATP and any other variations in signal intensity is expected to affect both (NAD metabolites and ATP) similarly, leaving the ratio unchanged and therefore comparable between measurements.

Quality of fit

CRLB was determined by Monte Carlo simulations[39,40] to assess the accuracy of the fitting. For this, complex Gaussian noise matching the SNR of acquired DEMz spectra was added to the fit. This noisy fit was then run again through the fitting algorithm after which the noise was added again to the fit. This procedure was repeated 100 times and the coefficient of variation between the fitted amplitudes was determined, resulting in CRLB.

CRLBs from NADH and NAD+ fits of FIDs and edited spectra acquired during normal perfusion were used as quantitative markers to judge the effectiveness of the DEMz sequence compared to a regular FID.

Statistics

The normal distribution of our data was verified by a Wilson Shapiro test. Subsequently, a two-sided paired student t-test was performed on the ischemia protocol data in young and healthy volunteers. Data from the comparison of NAD+ and NADH content in older adults was tested by an unpaired two-sided student *t*-test. Values are reported as mean ± standard error of the mean (SEM). Agreement between MRS measurements of NADH and NAD+ content and metabolomics were judged by linear correlation and the resulting R^2.

Reporting summary

Further information on research design is available in the Nature Portfolio Reporting Summary linked to this article.

Data availability

Screening data of the study in which exercise-trained versus normally active older volunteers were compared has been re-used from ref. 23, and can be found here: https://doi.org/10.1038/s41467-021-24956-2. This study was registered at clinicaltrials.gov with the identifier NCT03666013. All source data is provided with this paper in the source data file. Source data are provided in this paper.

References

1. Ortega, F. B., Lavie, C. J. & Blair, S. N. Obesity and cardiovascular disease. *Circ. Res.* **118**, 1752–1770 (2016).
2. Collaboration, N. C. D. R. F. Worldwide trends in body-mass index, underweight, overweight, and obesity from 1975 to 2016: a pooled analysis of 2416 population-based measurement studies in 128.9 million children, adolescents, and adults. *Lancet* **390**, 2627–2642 (2017).
3. Wild, S., Roglic, G., Green, A., Sicree, R. & King, H. Global prevalence of diabetes: estimates for the year 2000 and projections for 2030. *Diab. Care* **27**, 1047–1053 (2004).
4. Hesselink, M. K., Schrauwen-Hinderling, V. & Schrauwen, P. Skeletal muscle mitochondria as a target to prevent or treat type 2 diabetes mellitus. *Nat. Rev. Endocrinol.* **12**, 633–645 (2016).
5. Frederick, D. W. et al. Loss of NAD homeostasis leads to progressive and reversible degeneration of skeletal muscle. *Cell Metab.* **24**, 269–282 (2016).
6. Lowell, B. B. & Shulman, G. I. Mitochondrial dysfunction and type 2 diabetes. *Science* **307**, 384–387 (2005).
7. de Guia, R. M. et al. Aerobic and resistance exercise training reverses age-dependent decline in NAD(+) salvage capacity in human skeletal muscle. *Physiol. Rep.* **7**, e14139 (2019).
8. Kim, H. J. et al. Metabolomic analysis of livers and serum from high-fat diet induced obese mice. *J. Proteome Res.* **10**, 722–731 (2011).
9. Zhu, X. H., Lu, M., Lee, B. Y., Ugurbil, K. & Chen, W. In vivo NAD assay reveals the intracellular NAD contents and redox state in healthy human brain and their age dependences. *Proc. Natl Acad. Sci. USA* **112**, 2876–2881 (2015).
10. Massudi, H. et al. Age-associated changes in oxidative stress and NAD+ metabolism in human tissue. *PLoS ONE* **7**, e42357 (2012).
11. Janssens, G. E. et al. Healthy aging and muscle function are positively associated with NAD(+) abundance in humans. *Nat. Aging* **2**, 254–263 (2022).
12. Yoshino, J., Mills, K. F., Yoon, M. J. & Imai, S. Nicotinamide mononucleotide, a key NAD(+) intermediate, treats the pathophysiology of diet- and age-induced diabetes in mice. *Cell Metab.* **14**, 528–536 (2011).
13. Stein, L. R. & Imai, S. The dynamic regulation of NAD metabolism in mitochondria. *Trends Endocrinol. Metab.* **23**, 420–428 (2012).
14. Lu, M., Zhu, X. H. & Chen, W. In vivo (31) P MRS assessment of intracellular NAD metabolites and NAD(+) /NADH redox state in human brain at 4 T. *NMR Biomed.* **29**, 1010–1017 (2016).
15. De Graaf, R. A. et al. Detection of cerebral NAD(+) in humans at 7T. *Magn. Reson. Med.* **78**, 828–835 (2017).
16. Meyerspeer, M. et al. (31) P magnetic resonance spectroscopy in skeletal muscle: experts' consensus recommendations. *NMR Biomed.* **34**, e4246 (2020).
17. Hetherington, H. P., Spencer, D. D., Vaughan, J. T. & Pan, J. W. Quantitative (31)P spectroscopic imaging of human brain at 4 Tesla: assessment of gray and white matter differences of phosphocreatine and ATP. *Magn. Reson. Med.* **45**, 46–52 (2001).
18. De Graaf R. A. *In Vivo NMR Spectroscopy: Principles and Techniques.* (John Wiley & Sons, 2013).
19. Mescher, M., Merkle, H., Kirsch, J., Garwood, M. & Gruetter, R. Simultaneous in vivo spectral editing and water suppression. *NMR Biomed.* **11**, 266–272 (1998).
20. Sørensen, O. W., Rance, M. & Ernst, R. R. z Filters for purging phase- or multiplet-distorted spectra. *J. Magn. Reson. (1969)* **56**, 527–534 (1984).
21. Sahlin, K. NADH and NADPH in human skeletal muscle at rest and during ischaemia. *Clin. Physiol.* **3**, 477–485 (1983).
22. Poljsak B., Kovac V. & Milisav I. Healthy lifestyle recommendations: do the beneficial effects originate from NAD(+) amount at the cellular level? *Oxid. Med. Cell Longev.* https://doi.org/10.1155/2020/88196272020 (2020).
23. Grevendonk, L. et al. Impact of aging and exercise on skeletal muscle mitochondrial capacity, energy metabolism, and physical function. *Nat. Commun.* **12**, 4773 (2021).
24. Soderlund, K. & Hultman, E. ATP content in single fibres from human skeletal muscle after electrical stimulation and during recovery. *Acta Physiol. Scand.* **139**, 459–466 (1990).
25. Dziadosz, M. et al. Quantification of NAD(+) in human brain with (1) H MR spectroscopy at 3 T: comparison of three localization techniques with different handling of water magnetization. *Magn. Reson. Med.* **88**, 1027–1038 (2022).
26. Adriany, G. & Gruetter, R. A half-volume coil for efficient proton decoupling in humans at 4 tesla. *J. Magn. Reson.* **125**, 178–184 (1997).
27. van Zijl, P. C., Moonen, C. T. & von Kienlin, M. Homonuclear J refocusing in echo spectroscopy. *J. Magn. Reson. (1969)* **89**, 28–40 (1990).
28. Keeler J. Understanding NMR Spectroscopy. (Wiley, Chichester, England, 2005).
29. Sørensen, O. W., Eich, G. W., Levitt, M. H., Bodenhausen, G. & Ernst, R. R. Product operator formalism for the description of NMR pulse experiments. *Prog. Nucl. Magn. Reson. Spectrosc.* **16**, 163–192 (1984).
30. Kingsley, P. B. Product operators, coherence pathways, and phase cycling. Part II. Coherence pathways in multipulse sequences: spin echoes, stimulated echoes, and multiple-quantum coherences. *Concepts Magn. Reson.* **7**, 115–136 (1995).
31. Rance, M., Bodenhausen, G., Wagner, G., Wüthrich, K. & Ernst, R. R. A systematic approach to the suppression of J cross peaks in 2D exchange and 2D NOE spectroscopy. *J. Magn. Reson. (1969)* **62**, 497–510 (1985).
32. Dempster, P. & Aitkens, S. A new air displacement method for the determination of human body composition. *Med. Sci. Sports Exerc.* **27**, 1692–1697 (1995).
33. Siri, W. E. Body composition from fluid spaces and density: analysis of methods. *Nutrition* **9**, 480–91 (1961).
34. Schrauwen-Hinderling, V. B. et al. Impaired in vivo mitochondrial function but similar intramyocellular lipid content in patients with type 2 diabetes mellitus and BMI-matched control subjects. *Diabetologia* **50**, 113–120 (2007).
35. Bergstrom, J. Percutaneous needle biopsy of skeletal muscle in physiological and clinical research. *Scand. J. Clin. Lab Invest.* **35**, 609–616 (1975).
36. Conley, K. E., Ali, A. S., Flores, B., Jubrias, S. A. & Shankland, E. G. Mitochondrial NAD(P)H In vivo: identifying natural indicators of oxidative phosphorylation in the (31)P magnetic resonance spectrum. *Front. Physiol.* **7**, 45 (2016).
37. Lu, M., Zhu, X. H., Zhang, Y. & Chen, W. Intracellular redox state revealed by in vivo (31) P MRS measurement of NAD(+) and NADH contents in brains. *Magn. Reson. Med.* **71**, 1959–1972 (2014).
38. Bogner, W. et al. Assessment of (31)P relaxation times in the human calf muscle: a comparison between 3 T and 7 T in vivo. *Magn. Reson. Med.* **62**, 574–582 (2009).
39. Ratiney, H. et al. Time-domain semi-parametric estimation based on a metabolite basis set. *NMR Biomed.* **18**, 1–13 (2005).
40. Cavassila, S., Deval, S., Huegen, C., van Ormondt, D. & Graveron-Demilly, D. Cramer-Rao bound expressions for parametric estimation of overlapping peaks: influence of prior knowledge. *J. Magn. Reson.* **143**, 311–320 (2000).
41. Matsumura H. & Miyachi S. Cycling assay for nicotinamide adenine dinucleotides. *Methods Enzymol.* **69**, 465–470 (1980).
42. Remie, C. M. E. et al. Nicotinamide riboside supplementation alters body composition and skeletal muscle acetylcarnitine concentrations in healthy obese humans. *Am. J. Clin. Nutr.* **112**, 413–426 (2020).
43. Ritov, V. B., Menshikova, E. V. & Kelley, D. E. High-performance liquid chromatography-based methods of enzymatic analysis:

electron transport chain activity in mitochondria from human ske-letal muscle. *Anal. Biochem.* **333**, 27–38 (2004).

44. Blacker, T. S. & Duchen, M. R. Investigating mitochondrial redox state using NADH and NADPH autofluorescence. *Free Radic. Biol. Med.* **100**, 53–65 (2016).
45. Blacker, T. S. et al. Separating NADH and NADPH fluorescence in live cells and tissues using FLIM. *Nat. Commun.* **5**, 3936 (2014).
46. Guezennec, C. Y. et al. In situ NADH laser fluorimetry during muscle contraction in humans. *Eur. J. Appl. Physiol. Occup. Physiol.* **63**, 36–42 (1991).
47. de Graaf, R. A. & Behar, K. L. Detection of cerebral NAD(+) by in vivo (1)H NMR spectroscopy. *NMR Biomed.* **27**, 802–809 (2014).

Acknowledgements

Author contributions

J.M., R.G., and L.L. designed the sequence, and J.M. and L.L. imple-mented it. J.M., Y.B., R.M., L.G., and K.B. performed experiments, ana-lyzed data, and reviewed and edited the paper. M.H., P.S., J.H., L.L., and V.S. designed the study. J.W., M.H., P.S., J.H., R.H., M.B., R.G., L.L., and V.S. were involved in the interpretation of the data, and reviewed and edited the paper.

Competing interests

The authors declare no competing interests.

Additional information

Supplementary information The online version contains supplementary material available at https://doi.org/10.1038/s41467-024-53292-4.

Correspondence and requests for materials should be addressed to Vera B. Schrauwen-Hinderling.

Peer review information *Nature Communications* thanks Martin Krssak, Davy Sinnaeve, and the other, anonymous, reviewer(s) for their con-tribution to the peer review of this work. A peer review file is available.

Reprints and permissions information is available at http://www.nature.com/reprints

Publisher's note Springer Nature remains neutral with regard to jur-isdictional claims in published maps and institutional affiliations.